Optics Letters

Strongly confined atomic localization by Rydberg coherent population trapping

Teodora Kirova,[1] Ning Jia,[2,6] Seyyed Hossein Asadpour,[3] Jing Qian,[4,7] Gediminas Juzeliūnas,[5] and Hamid Reza Hamedi[5,8]

[1]Institute of Atomic Physics and Spectroscopy, University of Latvia, LV-1004, Latvia
[2]The Public Experimental Center, University of Shanghai for Science and Technology, Shanghai 200093, China
[3]Department of Physics, Iran University of Science and Technology, Tehran, Iran
[4]Department of Physics, School of Physics and Electronic Science, East China Normal University, Shanghai 200062, China
[5]Institute of Theoretical Physics and Astronomy, Vilnius University, Saulėtekio 3, LT-10257, Vilnius, Lithuania
[6]e-mail:jianing09@gmail.com
[7]e-mail: jqian1982@gmail.com
[8]e-mail: hamid.hamedi@tfai.vu.lt

Received 22 June 2020; revised 5 August 2020; accepted 14 August 2020; posted 14 August 2020 (Doc. ID 400849); published 24 September 2020

We investigate the possibility to attain strongly confined atomic localization using interacting Rydberg atoms in a coherent population trapping ladder configuration, where a standing-wave is used as a coupling field in the second leg of the ladder. Depending on the degree of compensation for the Rydberg level energy shift induced by the van der Waals interaction, by the coupling field detuning, we distinguish between two antiblockade regimes, i.e., a partial antiblockade (PA) and a full antiblockade. While a periodic pattern of tightly localized regions can be achieved for both regimes, the PA allows much faster convergence of spatial confinement, yielding a high-resolution Rydberg state-selective superlocalization regime for higher-lying Rydberg levels. In comparison, for lower-lying Rydberg levels, the PA leads to an anomalous change of spectra linewidth, confirming the importance of using a stable uppermost state to achieve a superlocalization regime.

https://doi.org/10.1364/OL.400849

The spatial confinement of atoms with high precision, e.g., atom localization, has been of continuous interest in quantum mechanics, while modern tools of quantum optics have made the actual realization of such experiments possible. The localization of an atom typically resorts to a measurement of the population, whether atoms are in the upper or ground state. Taking account of the parameters of atom–field interaction, as well as the internal states will lead to a suitable measurement for higher-precision localization. Current investigations have been driven by the possibility of practical applications, including nanolithography [1], laser cooling and trapping [2], and other areas of atomic physics [3].

A high-resolution localization scheme based on the phenomenon of coherent population trapping (CPT) [4] was initially proposed [5], where extreme localization of an atom passing through the standing-wave (SW) field can be achieved, while the localization resolution can be increased via changing the relative intensity of probe and SW fields. A variety of methods have been developed for subwavelength localization of atoms interacting with the SW fields, for example, via absorption [6,7], level population [8–10], spontaneously emitted photons [11], atom diffraction through a measurement induced grating [12], and using complex energy-level structure [13]. On the experimental side, using electromagnetically induced transparency (EIT) [14] with a SW coupling laser of sinusoidally varying intensity, atom and subwavelength atom localizations were reported by the Yavuz group [15,16] by utilizing the sensitivity of the atomic dark states.

On the other hand, many problems arise when it comes to possibilities to achieve localization of Rydberg atoms, due to the difficulty in confining them in a small region with high density. The strong van der Waals (vdW) interactions enhance the nonlinear properties of Rydberg media via the phenomenon of a dipole blockade [17] and open new opportunities for quantum optics and quantum information applications [18]. The latter makes the question of experimentally achievable precise localization of highly excited Rydberg atoms an important one. When the Rydberg level energy shift caused by the Rydberg–Rydberg interaction is compensated for by laser detuning, the phenomenon of so-called antiblockade occurs [19,20], which is later extensively used in different systems [21–23]. Since in our study the vdW interaction plays a main role, the corresponding antiblockade is a vdW-type Rydberg antiblockade, unlike the case of a dipole–dipole-type antiblockade, which happens when the dipole–dipole interaction is dominant [24].

In this work, we propose and analyze a theoretical scheme for the subwavelength Rydberg atom localization by applying a SW coupling field in a ladder scheme CPT configuration. We show that the Rydberg level energy shift due to the strong Rydberg–Rydberg interaction can be partially compensated for by a corresponding detuning [e.g., in the regime of partial

antiblockade (PA)], which under certain conditions leads to spatial confinement of the center of mass of the Rydberg atoms with precision down to subnanometer scale. In order to predict possible experimental realizations of the localization scheme, our numerical simulations are performed under realistic parameters for atomic ^{87}Rb.

We consider an ensemble of interacting Rydberg atoms in a ladder excitation scheme shown in Fig. 1. Each atom is in a three-level ladder configuration, where the ground $|g\rangle$ and middle $|m\rangle$ states are coupled by the probe field with Rabi frequency Ω_p, while the $|m\rangle$ and the Rydberg state $|r\rangle$ are connected via the coupling field $\Omega_s(x)$. The probe and coupling field detunings from the atomic $|g\rangle \to |m\rangle$ and $|m\rangle \to |r\rangle$ transitions are denoted by Δ_p and Δ_s, respectively. We will use the rotating wave approximation and assume a frozen-atom limit due to the fast operation of the experiments, typically on the order of μs [25]. The Hamiltonian of the atomic system then reads $H = H_a + H_{af} + U_{\mathrm{vdW}}$, where the constituting terms $H_a = \sum_j^N [\Delta_p \sigma_{mm}^j + \Delta_s \sigma_{rr}^j]$, $H_{af} = \sum_j^N [\Omega_p \sigma_{mg}^j + \Omega_s \sigma_{rm}^j + \mathrm{H.c.}]$, and $U_{\mathrm{vdW}} = \sum_{i<j}^N \frac{C_6}{|r_i - r_j|^6} \sigma_{rr}^i \sigma_{rr}^j$ describe, respectively, the unperturbed atomic dynamics, the atom–field coupling, and the inter-nuclear vdW interaction. Here the operator $\sigma_{\alpha\beta}^j = |\alpha\rangle\langle\beta| (\alpha \neq \beta)$ describes atomic transitions, and $\sigma_{\alpha\alpha}^j = |\alpha\rangle\langle\alpha|$ is the projection operator. Under the mean-field approximation, the time evolution of the jth atom operator $\sigma_{\alpha\beta}^j$ is governed by the equations

$$
\begin{aligned}
\dot{\sigma}_{gg}^j &= i\Omega_p \sigma_{gm}^j - i\Omega_p^* \sigma_{mg}^j + 2\gamma_{gm}\sigma_{mm}^j, \\
\dot{\sigma}_{rr}^j &= i\Omega_s \sigma_{mr}^j - i\Omega_s^* \sigma_{rm}^j, \\
\dot{\sigma}_{gm}^j &= (i\Delta_p - \gamma_{gm})\sigma_{gm}^j + i\Omega_p^* (\sigma_{gg}^j - \sigma_{mm}^j) + i\Omega_s \sigma_{gr}^j, \\
\dot{\sigma}_{gr}^j &= i(\Delta_s - s)\sigma_{gr}^j + i\Omega_s^* \sigma_{gm}^j - i\Omega_p^* \sigma_{mr}^j, \\
\dot{\sigma}_{mr}^j &= [i(\Delta_s - s - \Delta_p) - \gamma_{gm}]\sigma_{mr}^j \\
&\quad + i\Omega_s^* (\sigma_{mm}^j - \sigma_{rr}^j) - i\Omega_p \sigma_{gr}^j,
\end{aligned}
\tag{1}
$$

where $\Gamma_m = 2\gamma_{gm}$, $\gamma_{mr} = \gamma_{gm}$, $\gamma_{\alpha\beta} = (\Gamma_\alpha + \Gamma_\beta)/2[\alpha$, and $\beta \in (g, m, r)]$, with $\Gamma_m \gg \Gamma_r$. Here $\Gamma_{m(r)}$ is the spontaneous decay rate of the state $|m(r)\rangle$, while γ_{gm} represents the dephasing rate of the $|g\rangle \to |m\rangle$ atomic transition. The parameter s describes the energy shifts to the state $|r_j\rangle$ induced by the vdW interaction with other exciting atoms usually situated beyond the blockade radius R_b [26]. Under the steady-state condition $\dot{\sigma}_{\alpha\beta}(t) \equiv 0$, we can derive the analytical expression for the Rydberg level population σ_{rr}, following [27]:

$$
\sigma_{rr} = \frac{I_p(I_p + I_s)}{(I_p + I_s)^2 + 2\Delta_p(\Delta_s - s)I_s + (\Delta_s - s)^2(\gamma_{gm}^2 + \Delta_p^2 + 2I_p)},
\tag{2}
$$

where $I_{p/s} = |\Omega_{p/s}|^2$ represents the laser intensities. A more rigorous equality of intensity that differs by a constant coefficient $2c\epsilon_0\hbar^2/\mu^2$, with μ the electric dipole moment, is ignored without loss of generality. When $s = 0$ and $\Delta_p \ll \gamma_{gm}$, σ_{rr} forms a Lorenzian lineshape with a half-linewidth of single-atom Rydberg probability: $\omega = \frac{I_p + I_s}{\sqrt{\gamma_{gm}^2 + \Delta_p^2 + 2I_p}}$.

An atom in Rydberg state $|r\rangle^i$ would induce a vdW shift of level $|r\rangle^j$ in another atom separated by distance r, which effectively translates into a two-photon detuning. The vdW interaction then blocks the excitation of all the atoms for which this shift is much larger than w. The blockade radius can therefore be defined as $R_b = (C_6/\omega)^{\frac{1}{6}}$, where C_6 denotes the vdW coefficient. Only one atom can be excited within the blockade radius R_b, and the separation r between the two excited atoms meets the relation $r > R_b$, so it is reasonable to introduce a short-range cutoff to the spatial integral at R_b for describing the vdW interaction given by $s = \int_{R_b}^{\infty} \frac{C_6}{\mathbf{r^6}} \sigma_{rr}\rho \mathrm{d}^3\mathbf{r}$. Here $\sigma_{rr}\rho$ represents the density of excited atoms in the ensemble, ρ is the atomic density, $1/\rho = 4\pi R^3/3$ is the space occupied by a single atom, and R is the average interatomic spacing.

With the above equations in mind and assuming $\Delta_p = 0$, the magnitude of the approximated interaction s becomes $s = \frac{\omega}{\xi}\sigma_{rr} = \frac{I_p(I_p+I_s)^2}{\xi[(I_p+I_s)^2+{\Delta_s}^2(\gamma_{gm}^2+2I_p)]\sqrt{\gamma_{gm}^2+2I_p}}$, where in order to obtain σ_{rr}, we have used the assumption $s = 0$. Here $\xi = (R/R_b)^3$ is treated as an adjustable parameter controlled by the atomic density, and a value of $\xi \leq 1$ means that the full blockade is attainable. Let us consider that the coupling field is a SW in the $\hat{x}$ direction $\Omega_s(x) = \Omega_{s0}\sin(kx)$, with Ω_{s0} its peak amplitude and $k = 2\pi \sin\phi/\Lambda$ the wavevector, while the probe field is a traveling wave (TW). The SW can be produced by confining the field in an optical cavity or a Fabry–Perot resonator, or by using two counter-propagating laser beams.

According to Eq. (2), when the coupling-field detuning compensates for the vdW shift exactly by $\Delta_s = s$, the expression for the population simplifies to $\sigma_{rr} = I_p/[I_p + I_s(x)]$. A quick observation shows that at the nodes of the SW, i.e., $kx = n\pi$ $(n \in integers)$, the Rydberg state population can robustly persist $\sigma_{rr} \equiv 1$. Measuring the population in the Rydberg state results in a tight localization of the ensemble of Rydberg atoms. With the condition of $\Delta_s = s$, the system evolves into a spatially dependent dark state $|D\rangle = \frac{(\Omega_p|r\rangle - \Omega_s|g\rangle)}{\sqrt{\Omega_p^2+\Omega_s^2}}$, since the decay of the Rydberg state is negligible. The system adiabatically follows the dark state as x changes. It is easily seen that at the SW coupling field nodes, where $\Omega_s = 0$, the dark state reduces to the excited Rydberg state $|r\rangle$. Thus, the atom is excited to the Rydberg state via a smooth adiabatic change of $|D\rangle$ as $\Omega_s = \Omega_s(x)$

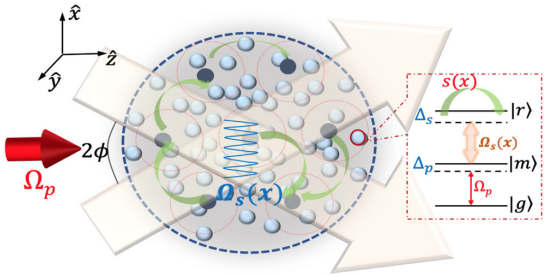

Fig. 1. Schematic representation of an atomic ensemble composed of numbers of blocked Rydberg superatoms that are coupled by a SW strong coupling field $\Omega_s(x)$ and a weak traveling wave (TW) probe field Ω_p. The SW field $\Omega_s(x)$ with a spatial period $\lambda = \Lambda/(2\sin\phi)$ is formed by two propagating fields with an angle 2ϕ symmetrically with respect to the $\hat{z}$ axis. Λ is the wavelength. The probe field Ω_p propagates along the $\hat{z}$ direction normal to the SW field. Inset shows a three-level atom ladder configuration. s describes the vdWs interacting energy between the interatomic Rydberg states.

passes through its zero points, and the population of $|r\rangle$ can be tightly localized. Hence the full antiblockade (FA) case is treated as $\Delta_s \equiv s(x)$. We also consider a PA regime in which only the Rydberg shifts at the field nodes are compensated for by $\Delta_s = s(x = n\pi/k)$. In reality, due to the space dependence of interactions, PA is more feasible. In the PA regime, the condition $\Delta_s = s(x = n\pi/k)$ can be simplified to the form $\Delta_s{}^3\xi(2I_p + \gamma_{gm}^2)^{3/2} + \Delta_s \xi I_p^2\sqrt{2I_p + \gamma_{gm}^2} - I_p^3 = 0$. By solving the cubic equation with respect to Δ_s and taking only the real root, we can obtain the value of the coupling field detuning that satisfies the PA condition, which is: $\Delta_s = \frac{2^{1/3}W^2 - 2\times 3^{1/3}\xi^2}{6^{2/3}\xi W} \frac{I_p}{\sqrt{\gamma_{gm}^2 + 2I_p}}$, where $W = (9\xi^2 + \sqrt{3\xi^4(4\xi^2 + 27)})^{1/3}$.

In order to explore the real performance of Rydberg localization via a SW, especially paying attention to the roles of FA and PA, we place the scheme in ^{87}Rb atoms where the levels $|g\rangle$, $|m\rangle$, $|r\rangle$ are represented by the actual $|5S_{1/2}\rangle$, $|5P_{3/2}\rangle$, $|60S_{1/2}\rangle$ states [28]. The dissipation is determined primarily by the decay rate of the excited state $|m\rangle$, given by $\gamma_{gm}/2\pi = 3.025$ MHz. While the amplitude of the coupling field Rabi frequency is fixed at $\Omega_{s0}/2\pi = 80$ MHz and the wavelength $\Lambda = 480$ nm, the continuous probe field has a Rabi frequency $\Omega_p = \Omega_{s0}/\kappa$, where $\kappa = \Omega_{s0}/\Omega_p$ describes the relative ratio of laser amplitudes, and the wavelength of 780 nm. The tunable coefficient κ in our calculations can take different values; however, in reality, a large κ value requires the probe beam to be very weak, which results in a significantly long time for reaching steady state. Due to the limited lifetime of the Rydberg states, we expect the best localization results to be achieved for an optimal κ, for which the time for the system to reach steady state denoted by T_s is 1/10 of the Rydberg states' lifetime. This leaves sufficient time for a stable localization measurement in the experiment. For example, the $|r\rangle = |60S_{1/2}\rangle$ lifetime is 226.86 μs, leading to $T_s = 22.68$ μs. Note that T_s is increased for larger κ values, as T_s depends on the absolute values of the Rabi frequencies. Since T_s is restrained by the Rydberg level lifetime, it is necessary to find out a best κ value for spatially localizing the atoms.

For estimating the optimal κ values, we plot in Fig. 2 the κ-T_s relation by directly solving the equations of motion (1). For comparison we also introduce a lower-lying Rydberg level $|r\rangle = |30s_{1/2}\rangle$ with its lifetime about 26.6 μs, giving $T_s = 2.66$ μs for a steady localization. A transition of $|5S_{1/2}\rangle \to |5P_{1/2}\rangle \to |30S_{1/2}\rangle$ is also possible in practice [29]. In Fig. 2(a), it is clear that in the case of FA, a steady localization can be ensured by $\kappa = 236$ and $\kappa = 80$ for Rydberg energy levels $|r\rangle = |60S_{1/2}\rangle$ and $|30S_{1/2}\rangle$, respectively, as highlighted by green dots. Changing the atomic density ξ does not affect the steady time T_s. The detailed transient responses are shown in the insets. Shown in Fig. 2(b) for the PA regime, a smaller ξ (equivalent to a stronger atomic density), increases the time T_s due to the imperfect energy-shift compensation. Hence, the optimal κ has to be significantly reduced to reach the same T_s, which may cause broadening of localization peaks, as confirmed by Fig. 4(c).

Next, in order to elucidate the role of the atomic density ξ, we study quantitatively the distribution of the blocked energy s in space. Figure 3(a) illustrates the dependence of Δ_s on ξ and for different optimal κ values, as obtained by Fig. 2. Intuitively, Δ_s decreases with ξ because a bigger atomic density with $R > R_b$ would cause the interatomic interaction to be

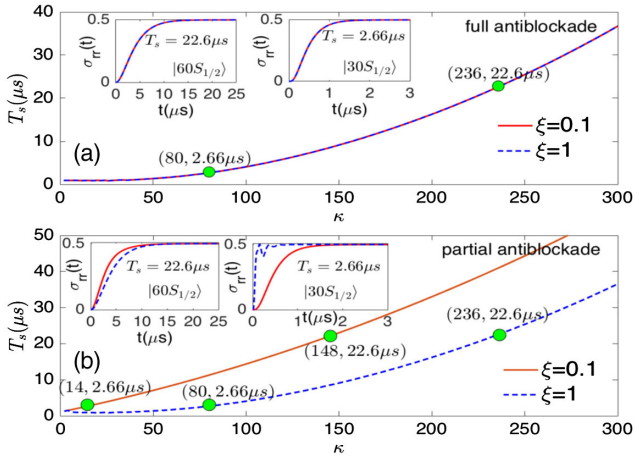

Fig. 2. Relation between the steady-state time T_s and κ for the Rydberg energy levels $|r\rangle = |60S_{1/2}\rangle$ and $|30S_{1/2}\rangle$ in the cases of (a) FA: $\Delta_s \equiv s$ and (b) PA: $\Delta_s = s(x = n\pi/k)$. Different ξ values are comparably displayed for $\xi = 0.1$ (red solid) and $\xi = 1.0$ (blue dotted). Insets show the transient response of population $\sigma_{rr}(t)$ for two real Rydberg levels, accordingly.

weaker. Moreover, a larger κ is accompanied by a smaller Ω_p, lowering the Rydberg-state probability, the same as the Rydberg shift s. Figures 3(b) and 3(c) show the spatial dependence of the Rydberg shifted energy $s(x)$. Except that $s(x)$ is significantly decreased if κ is enhanced due to a weaker probe intensity, it is clear that a smaller $\xi(= 0.1)$ causes a large dip at the localized points $x = n\pi/k$ of the spatial profile of s. For the case with $|60S_{1/2}\rangle$ and in the regime of PA, as shown in (c) [blue dashed curve], the shift s is overcome by a suitable two-photon detuning Δ_s at the nodes $x = n\pi/k$, resulting in an effective two-photon resonance at those positions. Yet, out of the nodes $x \neq n\pi/k$, s sustains a higher level that cannot be overcome by Δ_s, causing the steady solution σ_{rr} to decrease significantly. The role of PA is not dominant if ξ is larger (e.g., $\xi = 1$, red solid curve), as in this case when the energy s remains almost the same for all positions $x = n\pi/k$ and $x \neq n\pi/k$. On the other hand, the FA regime can self-consistently compensate for the shifted energy $s(x)$ at all spatial positions x, preventing improving the spectra linewidth by different atomic densities.

Figure 4 presents the simulations of the state-selective localization protocol by measuring the population distribution of the

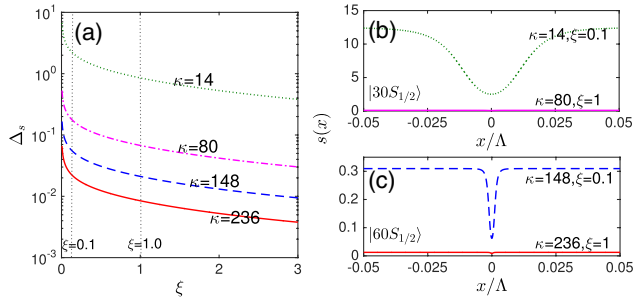

Fig. 3. (a) Relation of Δ_s and ξ for values of κ for the Rydberg energy levels $|r\rangle = |60S_{1/2}\rangle$ or $|30S_{1/2}\rangle$ determined by Fig. 2. (b), (c) Relation of the Rydberg shift s and position x for $\xi = 0.1$ and $\xi = 1.0$ for the corresponding κ: (b) Rydberg energy level $|r\rangle = |30S_{1/2}\rangle$; (c) Rydberg energy level $|r\rangle = |60S_{1/2}\rangle$. γ_{gm} is treated as the frequency unit.

Rydberg state. Clearly seen is the effect of the two parameters κ and ξ, as well as the difference between the FA and PA regimes. Adopting the optimal κ value $\kappa = 236$ for $|60S_{1/2}\rangle$, as obtained by Fig. 2, the Rydberg population σ_{rr} reaches its maximal value of 1.0 at the notes of SW, creating a periodic pattern of tightly localized regions for both PA and FA regimes. While $\xi = 1$ leads to matching of the localization lines in both regimes, as shown in Fig. 4(b) (because the energy s remains almost the same for all positions), the PA regime improves the spatial confinement significantly by reducing the spectral linewidth with respect to the FA when $\xi = 0.1$ [see Fig. 4(a)].

The reason could be understood as follows. For the case of FA by using the condition $\Delta_s \equiv s(x)$ in Eq. (2), we obtain $\sigma_{rr}^{\mathrm{FA}} = 1/(1 + \kappa^2 \sin^2(kx))$, where we have included the spatial dependence of the coupling field as $\Omega_s(x) = \Omega_{s0}\sin(kx)$. At the same time, the full width at half maxima (FWHM) of the localization spectral lines is given by $a^{\mathrm{FA}} = \arcsin(1/\kappa)\Lambda/\pi$, leading to 0.647 nm for the parameters in Fig. 4(a). For the case of PA, we can make only numerical estimates, giving a FWHM of 0.56 nm. If considering a lower-lying Rydberg state $|r\rangle = |30s_{1/2}\rangle$, the localization is accompanied by a broadening of the spectral linewidths, e.g., the localization peak is not as sharp with respect to the case with the higher-lying Rydberg state $|r\rangle = |60s_{1/2}\rangle$, as depicted in Figs. 4(c) and 4(d). Moreover, an anomalous behavior of spectra linewidth is observed now between the FA and PA regimes, i.e., the localization peaks are wider now for the PA regime, with a FWHM of σ_{rr} as wide as 5.93 nm. This could be due to the wider variation of interaction energy s around the localization points [see Fig. 3(b), dotted green line]. Such a comparison confirms the importance of using a stable uppermost state to achieve a superlocalization regime.

In conclusion, we study the possibility to achieve strong localization of interacting Rydberg atoms arranged in a three-level ladder CPT configuration using a TW probe and SW coupling fields. We distinguish between two antiblockade regimes, FA and PA, in which the detuning of the coupling field compensates for the Rydberg energy shift induced by the vdW interaction fully or partially, only at the nodes of the SW field. The sharpest Rydberg state-selective localization is achieved under the PA condition, when utilizing a higher-lying Rydberg level can give 100% population at the SW nodes, along with a FWHM below 1 nm. The spatial confinement is possible also when considering a lower shorter-lived Rydberg state, which is accompanied by a spectral line widening and a loss of the localization sharpness. Our findings are relevant in the emerging field of subnanometer localization of atoms [30], bringing us one step closer to novel applications in optical microscopy techniques in real experiments. Future investigations of the subwavelength atom localization are planned to involve more complicated level configurations, and will address the situations when multiple laser fields carrying orbital angular momentum are applied.

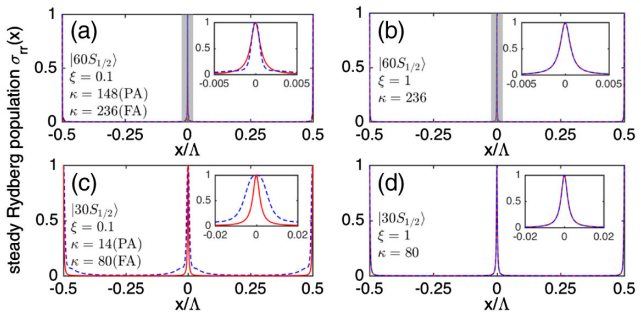

Fig. 4. Steady-state Rydberg population as a function of x/Λ with parameters: $\Omega_{s0}/2\pi = 80$ MHz, $\Omega_p = \Omega_{s0}/\kappa$, $\gamma_{gm}/2\pi = 3.025$ MHz, $\Delta_p = 0$. Red lines, FA ($\Delta_s \equiv s(x)$); blue dashed lines, PA under the condition $\Delta_s = s(x = n\pi/k)$. Parameters ξ and κ are described in the figure. Insets show a zoom-in around $x/\Lambda = 0$, clearly showing the difference between the two cases.

Funding. National Natural Science Foundation of China (11104076, 11474094); Science and Technology Commission of Shanghai Municipality (18ZR1412800); Short Term Scientific Mission (COST Action CA16221); Lithuanian Research Council Grant No. (S-MIP-20-36).

Disclosures. The authors declare no conflicts of interest.

REFERENCES

1. A. N. Boto, P. Kok, D. S. Abrams, S. L. Braunstein, C. P. Williams, and J. P. Dowling, Phys. Rev. Lett. **85**, 2733 (2000).
2. W. D. Phillips, Rev. Mod. Phys. **70**, 721 (1998).
3. C. S. Adams, M. Sigel, and J. Mlynek, Rev. Rep. **240**, 143 (1994).
4. E. Arimondo, Prog. Opt. **35**, 257 (1996).
5. G. S. Agarwal and K. T. Kapale, J. Phys. B **39**, 3437 (2006).
6. D. Zhang, R. Yu, Z. Sun, C. Ding, and M. S. Zubairy, J. Phys. B **52**, 035502 (2019).
7. B. Groisman, S. Popescu, and A. Winter, Phys. Rev. A **72**, 032317 (2005).
8. E. Paspalakis and P. L. Knight, Phys. Rev. A **63**, 065802 (2001).
9. V. Ivanov and Y. Rozhdestvensky, Phys. Rev. A **81**, 033809 (2010).
10. J. Mompart, V. Ahufinger, and G. Birk, Phys. Rev. A **79**, 053638 (2009).
11. F. Ghafoor, Phys. Rev. A **84**, 063849 (2011).
12. S. Kunze, K. Dieckmann, and G. Rempe, Phys. Rev. Lett. **78**, 2038 (1997).
13. H. R. Hamedi and G. Juzeliūnas, Phys. Rev. A **94**, 013842 (2016).
14. S. E. Harris, J. E. Field, and A. Imamoğlu, Phys. Rev. Lett. **64**, 1107 (1990).
15. J. A. Miles, Z. J. Simmons, and D. D. Yavuz, Phys. Rev. X **3**, 031014 (2013).
16. J. A. Miles, D. Das, Z. J. Simmons, and D. D. Yavuz, Phys. Rev. A **92**, 033838 (2015).
17. M. D. Lukin, M. Fleischhauer, R. Côté, L. M. Duan, D. Jaksch, J. I. Cirac, and P. Zoller, Phys. Rev. Lett. **87**, 037901 (2001).
18. M. Saffman, T. G. Walker, and K. Mölmer, Rev. Mod. Phys. **82**, 2313 (2010).
19. C. Ates, T. Pohl, T. Pattard, and J. M. Rost, Phys. Rev. Lett. **98**, 023002 (2007).
20. T. Amthor, C. Giese, C. S. Hofmann, and M. Weidemüller, Phys. Rev. Lett. **104**, 013001 (2010).
21. Z. Zuo and K. Nakagawa, Phys. Rev. A **82**, 062328 (2010).
22. T. E. Lee, H. Häffner, and M. C. Cross, Phys. Rev. Lett. **108**, 023602 (2012).
23. W. Li, C. Ates, and I. Lesanovsky, Phys. Rev. Lett. **110**, 213005 (2013).
24. S.-L. Su, "Rydberg antiblockade with resonant dipole-dipole interactions," arXiv:2006.06529v2 (2020).
25. A. Browaeys, D. Barredo, and T. Lahaye, J. Phys. B **49**, 152001 (2016).
26. D. Tong, S. M. Farooqi, J. Stanojevic, Y. P. Zhang, R. Côté, E. E. Eyler, and P. L. Gould, Phys. Rev. Lett. **93**, 063001 (2004).
27. D. Ma, D. Yu, X.-D. Zhao, and J. Qian, Phys. Rev. A **99**, 033826 (2019).
28. J. D. Pritchard, D. Maxwell, A. Gauguet, K. J. Weatherill, M. P. A. Jones, and C. S. Adams, Phys. Rev. Lett. **105**, 193603 (2010).
29. J. Han, T. Vogt, and W. Li, Phys. Rev. A **94**, 043806 (2016).
30. C. R. Copeland, J. Geist, C. D. McGray, V. A. Aksyuk, J. A. Liddle, B. R. Ilic, and S. M. Stavis, Light Sci. Appl. **7**, 31 (2018).